Progress In Electromagnetics Research B, Vol. 16, 155–188, 2009

PROPAGATION IN A HELICAL WAVEGUIDE WITH INHOMOGENEOUS DIELECTRIC PROFILES IN RECTANGULAR CROSS SECTION

Z. Menachem and M. Haridim

Department of Communication Engineering
Holon Institute of Technology
52 Golomb Street, POB 305, Holon 58102, Israel

Abstract—This paper presents a rigorous approach for the propagation of electromagnetic (EM) fields along a helical waveguide with arbitrary profiles in the rectangular cross section. The main objective is to develop a mode model to provide a numerical tool for the calculation of the output fields, output power density, and output power transmission for an arbitrary step's angle and the radius of the cylinder of the helical waveguide. Another objective is to demonstrate the ability of the model to solve practical problems with inhomogeneous dielectric profiles. The method is based on Fourier coefficients of the transverse dielectric profile and those of the input wave profile. Laplace transform is necessary to obtain the comfortable and simple input-output connections of the fields. This model is useful for the analysis of dielectric waveguides in the microwave and the millimeter-wave regimes, for diffused optical waveguides in integrated optics. The output power transmission and the output power density are improved by increasing the step's angle or the radius of the cylinder of the helical waveguide, especially in the cases of space curved waveguides.

1. INTRODUCTION

Various methods for the analysis of curved waveguides have been studied in the literature. The propagation of general-order modes in curved rectangular waveguide examined by using asymptotic expansion method [1]. A matrix formulation of the generalized telegraphist's equation [2] used to obtain a general set of equations for a guide of arbitrary cross section with curved axis. The matrix elements

Corresponding author: Z. Menachem (zionm@post.tau.ac.il).

involved mode-coupling coefficients which were obtained as rather general integrals of the mode basis functions and the space variables. Asymptotic forms of the coupling coefficients for gentle bends were determined and applied to propagation in rectangular guide bent into an arc of a circle between two sections of straight guide. For very sharp bends the matrix equations are tackled directly and results calculated numerically by truncation of the matrices at third order. By comparison with truncation at first and second order it seems that third order truncation should yield accurate numerical results.

Slabs with more general refractive index distributions were considered by Heiblum and Harris [3] and by Kawakami, Miyagi and Nishida [4], using a WKB method [5]. These two papers consider the case when the mode on the curved waveguide is not a small perturbation of a mode on the straight guide, but was guided essentially by the outer boundary. The modes of this nature are known as "edge-guided" modes. The increase in radiation losses due to curvature for slightly leaky modes on hollow dielectric or imperfect metallic waveguides, a sort of composite of open and closed waveguide behavior, was investigated by Marcatily and Schmeltzer [6].

Several methods of investigation of propagation were developed for study of empty curved waveguide and bends [7–10]. The results of precise numerical computations and extensive analytical investigation of the angular propagation constants were presented for various electromagnetic modes which may exit in waveguide bends of rectangular cross section [7]. A new equivalent circuit for circular E-plane bends, suitable for any curvature radius and rectangular waveguide type was presented in Ref. [8]. An accurate and efficient method of moments solution together with a mode-matching technique for the analysis of curved bends in a general parallel-plate waveguide was described in the case of a rectangular waveguides [9]. A rigorous differential method describing the propagation of an electromagnetic wave in a bent waveguide was presented in Ref. [10].

An analytical method to study a general helix-loaded structure has been published in Ref. [11]. The inhomogeneously-loaded helix enclosed in a cylindrical waveguide operating in the fast-wave regime. The tape-helix model has been used which takes into account the effect of the space-harmonics, and is used particularly in the cases that the structure is operated at high voltages and for high helix pitch angles. The propagation characteristics of an elliptical step-index fiber with a conducting helical winding on the core-cladding boundary [12] are investigated analytically where the coordinate systems are chosen for the circular and elliptical fibers. In their waveguides the core and the cladding regions are assumed to have constant real refractive indices

n_1 and n_2, where $n_1 > n_2$. The fibers are referred to as the elliptical helically cladded fiber and the circular helically cladded fiber.

An extensive survey of the related literature can be found in the book on electromagnetic waves and curved structures [13]. Propagation in curved rectangular waveguides by the perturbation techniques was introduced for a guide of cross section $a \times b$ whose axis was bent to radius R. Likewise, the twisted coordinate system with application to rectangular waveguides was introduced in Ref. [13]. The other chapters were concerned with curved guides, both rectangular and circular. Calculations were performed for the propagation coefficient, reflection, mode-conversion, mode-coupling and eigenfunctions for a variety of configurations by the asymptotic method. The radiation from curved open structures is mainly considered by using a perturbation approach, that is by treating the curvature as a small perturbation of the straight configuration. The perturbation approach is not entirely suited for the analysis of relatively sharp bends, such as those required in integrated optics and especially short millimeter waves.

An approximate method for predicting the field profile in a curved dielectric waveguide of rectangular cross section was described in [14]. For simplicity, the dielectric and free-space regions were treated separately. Inside the dielectric waveguide, the transverse field was expressed as an Airy function via a conformal transformation. For away from the guide, the field was expressed in terms of Hankel function of the second kind. This model can be applied to guiding structures of rectangular cross section where the transverse propagation constants can be obtained independently.

A theoretical mode model was developed in [15] to solve practical problems for a curved dielectric waveguide (approximately a plane curve) with a rectangular cross section. This model was a generalization of the method from the straight waveguide [16] also for a curved dielectric waveguide with a rectangular cross section where the calculations are dependent on the radius of the curvature, but on the small step's angle (δ_p) of the helical waveguide.

The main objective of this paper is to generalize the numerical mode model [15] from a curved dielectric waveguide (approximately a plane curve) with a rectangular cross section to a helical waveguide (a space curved waveguide for an arbitrary value of the step's angle and the radius of the cylinder of the helical waveguide) with a rectangular cross section. Another objective is to demonstrate the ability of the model to solve practical problems with inhomogeneous dielectric profiles in the cross section. This model has been applied in the case of a helical waveguide with arbitrary profiles in the cross section. The

generalized mode model with the two above objectives provides us a numerical tool for the calculation of the output fields and output power transmission for an arbitrary step's angle (δ_p) of the helical waveguide. The method is based on Fourier coefficients of the transverse dielectric profile and those of the input wave profile. This model is useful for the analysis of dielectric waveguides in the microwave and the millimeter-wave regimes, for diffused optical waveguides in integrated optics. Note that in our method, we do not consider the bending as a perturbation. The purpose of this study was to develop transfer relations between the wave components at the output and input ports of such waveguides as matrix functions of their dielectric profiles. The following sections present the formulation and the derivation of this method for a helical waveguide with arbitrary dielectric profile in the cross section as function of the step's angle (δ_p) and the radius of the cylinder (R) of the helical waveguide. The output power transmission is improved by increasing the step's angle or the radius of the cylinder of the helical waveguide, especially in the cases of space curved waveguides.

2. FORMULATION OF THE PROBLEM

The main objective of this paper is to generalize the numerical mode model [15] from a curved dielectric waveguide (approximately a plane curve) with a rectangular cross section to a helical waveguide (a space curved waveguide for an arbitrary value of the step's angle and the radius of the cylinder of the helical waveguide) with a rectangular cross section.

Figure 1 shows the geometry of the helical waveguide with a rectangular cross section. The direction of the wave propagation is along the axis of the helical waveguide. The axis of the helical waveguide is shown in Fig. 2(a). The deployment of the helix is shown in Fig. 2(b), where R is the radius of the cylinder, and δ_p is the step's angle. We start by finding the metric coefficients from the helical transformation of the coordinates. The latters will be used in the wave equations as will be outlined in the next section.

The helical transformation of the coordinates is achieved by two rotations and one translation, and is given in the form:

$$\begin{pmatrix} X \\ Y \\ Z \end{pmatrix} = \begin{pmatrix} \cos(\phi_c) & -\sin(\phi_c) & 0 \\ \sin(\phi_c) & \cos(\phi_c) & 0 \\ 0 & 0 & 1 \end{pmatrix} \begin{pmatrix} 1 & 0 & 0 \\ 0 & \cos(\delta_p) & -\sin(\delta_p) \\ 0 & \sin(\delta_p) & \cos(\delta_p) \end{pmatrix} \begin{pmatrix} x \\ 0 \\ y \end{pmatrix} + \begin{pmatrix} R\cos(\phi_c) \\ R\sin(\phi_c) \\ \zeta\sin(\delta_p) \end{pmatrix} = \begin{pmatrix} (R+x)\cos(\phi_c) + y\sin(\delta_p)\sin(\phi_c) \\ (R+x)\sin(\phi_c) - y\sin(\delta_p)\cos(\phi_c) \\ y\cos(\delta_p) + \zeta\sin(\delta_p), \end{pmatrix}, \quad (1)$$

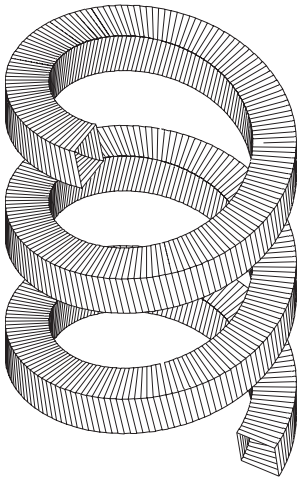

Figure 1. The rectangular helical waveguide.

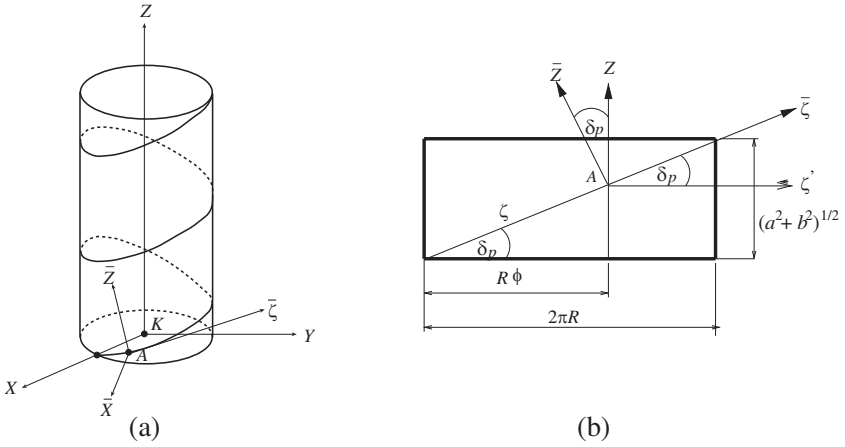

Figure 2. (a) Rotations and translation of the orthogonal system $(\overline{X}, \overline{\zeta}, \overline{Z})$ from point A to the orthogonal system (X, Y, Z) at point K. (b) Deployment of the helix.

where ζ is the coordinate along the axis of the helical waveguide, R is the radius of the cylinder, δ_p is the step's angle of the helical waveguide (see Figs. 2(a) and 2(b)), and $\phi_c = (\zeta \cos(\delta_p)/R$. Likewise, $0 \leq x \leq a$ and $0 \leq y \leq b$, where a and b are the dimensions in the cross section of the helical waveguide. Note that $\zeta \sin(\delta_p) = R\phi_c \tan(\delta_p)$.

Figure 2(a) shows the rotations and translation of the orthogonal

system $(\overline{X}, \overline{\zeta}, \overline{Z})$ from point A to the orthogonal system (X, Y, Z) at point K. In the first rotation, the $\overline{\zeta}$ and $\overline{Z}$ axes rotate around the $\overline{X}$ axis of the orthogonal system $(\overline{X}, \overline{\zeta}, \overline{Z})$ at the point A, until the $\overline{Z}$ axis becomes parallel to the Z axis $(\overline{Z} \parallel Z)$, and the $\overline{\zeta}$ axis becomes parallel to the X, Y plane $(\overline{\zeta} \parallel (X, Y))$ of the orthogonal system (X, Y, Z) at the point K. In the second rotation, the $\overline{X}$ and $\overline{\zeta}$ axes rotate around the $\overline{Z}$ axis $(\overline{Z} \parallel Z)$ of the orthogonal system $(\overline{X}, \overline{\zeta}, \overline{Z})$ until $\overline{X} \parallel X$ and $\overline{\zeta} \parallel Y$. After the two above rotations, we have one translation from the orthogonal system $(\overline{X}, \overline{\zeta}, \overline{Z})$ at point A to the orthogonal system (X, Y, Z) at the point K.

Figure 2(b) shows the deployment of the helix depicted in Fig. 2(a). The condition for the step's angle δ_p is given according to

$$\tan(\delta_p) \geq \frac{\sqrt{a^2 + b^2}}{2\pi R}, \tag{2}$$

where the dimensions in the cross section are denoted as a and b, and the radius of the cylinder is denoted as R.

The metric coefficients in the case of the helical waveguide according to Eq. (1) are:

$$h_x = 1, \tag{3a}$$

$$h_y = 1, \tag{3b}$$

$$\begin{aligned} h_\zeta &= \sqrt{\left(1 + \frac{x}{R}\right)^2 \cos^2(\delta_p) + \sin^2(\delta_p)\left(1 + \frac{y^2}{R^2}\cos^2(\delta_p)\right)} \\ &= \sqrt{1 + \frac{2x}{R}\cos^2(\delta_p) + \frac{x^2}{R^2}\cos^2(\delta_p) + \frac{y^2}{R^2}\cos^2(\delta_p)\sin^2(\delta_p)} \\ &\simeq 1 + \frac{x}{R}\cos^2(\delta_p). \end{aligned} \tag{3c}$$

Furthermore, the third and the fourth terms in the root of the metric coefficient h_ζ are negligible in comparison to the first and the second terms when $(x/R)^2 \ll 1$ and $(y/R)^2 \ll 1$. Nonetheless, the metric coefficient h_ζ still depends on δ_p, the step's angle of the helix (Fig. 2(b)). Note that the metric coefficient h_ζ is a function of x and y, which causes a difficulty in the separation of variables. Thus, the analytical methods are not suitable for the helical or the curved waveguide. The separation of variables is performed in this study, as a numerical method.

For small values of the step's angle δ_p $(\sin(\delta_p) \simeq \tan(\delta_p) \simeq \delta_p, \cos(\delta_p) \simeq 1)$, Condition (2) becomes $\delta_p \geq \sqrt{a^2 + b^2}/(2\pi R)$. For

small values of the step's angle, the helical waveguide becomes a curved waveguide, where the radius of the curvature of the helical waveguide can then be approximately by the radius of the cylinder ($\rho \simeq R$). In this case, the curved system (x, y, ζ) in conjunction with the curved waveguide is shown in Fig. 3, and the transformation of the Coordinates (1) is given as a special case of the curved transformation of the coordinates, as follows

$$X = (R + x)\cos\left(\frac{\zeta}{R}\right), \quad Y = (R + x)\sin\left(\frac{\zeta}{R}\right), \quad Z = y, \tag{4}$$

and the metric coefficients are given by

$$h_x = 1, \quad h_y = 1, \quad h_\zeta = 1 + \frac{x}{R}. \tag{5}$$

By using the Serret-Frenet relations for a spatial curve, we can find the curvature (κ) and the torsion (τ) for each spatial curve that is characterized by $x =$ constant and $y =$ constant for each pair (x, y) in the range. This is achieved by using the helical transformation introduced in Eq. (1). The curvature and the torsion (see Appendix A) are constants for constant values of the radius of the cylinder (R), the step's angle (δ_p) and the parameters (x, y) of the cross section. The curvature and the torsion are given by

$$\kappa = \frac{\sqrt{1 + C_t}}{R(1 + \tan^2(\delta_p) + C_t)}, \quad \tau = \frac{\tan(\delta_p)}{R(1 + \tan^2(\delta_p) + C_t)}, \tag{6}$$

where

$$C_t = \frac{x^2}{R^2} + 2\frac{x}{R} + \frac{y^2}{R^2}\sin^2(\delta_p).$$

The radius of curvature and the radius of torsion are given by $\rho = 1/\kappa$, and $\sigma = 1/\tau$, respectively. For small values of the step's angle ($\delta_p \ll 1$), the helical waveguide becomes a curved waveguide (Fig. 3), where the radius of the curvature of the helical waveguide can then be approximately by the radius of the cylinder ($\rho \simeq R$).

The generalization of the method from a curved dielectric waveguide [15] (approximately a plane curve) to a helical waveguide (a space curved waveguide for an arbitrary value of the step's angle of the helical waveguide) is presented in the following derivation. The derivation is based on Maxwell's equations for the computation of the EM field and the radiation power density at each point during propagation along a helical waveguide, with arbitrary profiles in the rectangular cross section. The method is based on Fourier coefficients

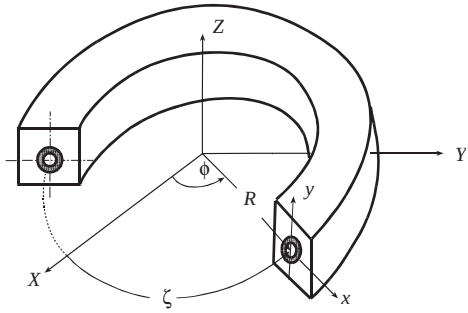

Figure 3. A general scheme of the curved coordinate system (x, y, ζ).

of the transverse dielectric profile and those of the input wave profile. The purpose of this study is to develop transfer relations between the wave components at the output and input ports of such helical waveguides as matrix functions of their dielectric profiles. Note that in our method, we do not consider the bending as a perturbation.

3. SOLUTION OF THE WAVE EQUATIONS

We assume that for most materials, the permeability μ is equal to that of free space ($\mu = \mu_0$). The wave equations for the electric and magnetic field components in the inhomogeneous dielectric medium $\epsilon(x, y)$ are given by

$$\nabla^2\mathbf{E} + \omega^2\mu\epsilon\mathbf{E} + \nabla\left(\mathbf{E}\cdot\frac{\nabla\epsilon}{\epsilon}\right) = 0, \tag{7a}$$

and

$$\nabla^2\mathbf{H} + \omega^2\mu\epsilon\mathbf{H} + \frac{\nabla\epsilon}{\epsilon}\times(\nabla\times\mathbf{H}) = 0, \tag{7b}$$

respectively. The transverse dielectric profile $(\epsilon(x, y))$ is defined as $\epsilon_0(1 + \chi_0 g(x, y))$, where ϵ_0 represents the vacuum dielectric constant, $g(x, y)$ is its profile function in the waveguide, and χ_0 is the susceptibility of the dielectric material. The normalized transverse derivatives of the dielectric profile $g(x, y)$ are defined as $(1/\epsilon(x, y))[(\partial/\partial x)\epsilon(x, y)]$ and $(1/\epsilon(x, y))[(\partial/\partial y)\epsilon(x, y)]$, respectively. From the helical transformation of Eq. (1), we can derive the Laplacian of the vector $\mathbf{E}$ (i.e., $\nabla^2\mathbf{E}$), and obtain the wave equations for the electric and magnetic fields in the inhomogeneous dielectric medium. It is necessary to find the values of $\nabla\cdot\mathbf{E}$, $\nabla(\nabla\cdot\mathbf{E})$, $\nabla\times\mathbf{E}$, and

$\nabla \times (\nabla \times \mathbf{E})$ in order to obtain the value of $\nabla^2\mathbf{E}$, where $\nabla^2\mathbf{E} = \nabla(\nabla \cdot \mathbf{E}) - \nabla \times (\nabla \times \mathbf{E})$. All these values are dependent on the metric Coefficients (3a)–(3c).

The components of $\nabla^2\mathbf{E}$ are given by

$$(\nabla^2\mathbf{E})_x = \nabla^2 E_x - \frac{1}{R^2 h_\zeta^2}\cos^2(\delta_p)E_x - 2\frac{1}{Rh_\zeta^2}\cos^2(\delta_p)\frac{\partial}{\partial\zeta}E_\zeta, \quad (8a)$$

$$(\nabla^2\mathbf{E})_y = \nabla^2 E_y, \quad (8b)$$

$$(\nabla^2\mathbf{E})_\zeta = \nabla^2 E_\zeta - \frac{1}{R^2 h_\zeta^2}\cos^2(\delta_p)E_\zeta + 2\frac{1}{Rh_\zeta^2}\cos^2(\delta_p)\frac{\partial}{\partial\zeta}E_x, \quad (8c)$$

where

$$\nabla^2 = \frac{\partial^2}{\partial x^2} + \frac{\partial^2}{\partial y^2} + \frac{1}{h_\zeta^2}\frac{\partial^2}{\partial\zeta^2} + \frac{1}{Rh_\zeta}\cos^2(\delta_p)\frac{\partial}{\partial x}, \quad (9)$$

and for $h_\zeta = 1 + (x/R)\cos^2(\delta_p)$. The derivation of Eqs. (8a)–(8c) is given in detail in Appendix B. The wave Eqs. (7a) and (7b) are written in the form

$$(\nabla^2\mathbf{E})_i + k^2 E_i + \partial_i(E_x g_x + E_y g_y) = 0, \quad (10a)$$

$$(\nabla^2\mathbf{H})_i + k^2 H_i + \partial_i(H_x g_x + H_y g_y) = 0, \quad (10b)$$

where $i = x, y, \zeta$. The local wavenumber parameter is given by $k = \omega\sqrt{\mu\epsilon(x,y)} = k_0\sqrt{1 + \chi_0 g(x,y)}$, and the free-space wavenumber is given by $k_0 = \omega\sqrt{\mu_0\epsilon_0}$. The expression $(\nabla^2\mathbf{E})_x$, for instance, is given according to Eq. (8a).

The transverse Laplacian operator is defined as

$$\nabla_\perp^2 = \nabla^2 - \frac{1}{h_\zeta^2}\frac{\partial^2}{\partial\zeta^2}. \quad (11)$$

The metric coefficient h_ζ is a function of x, thus we defined

$$h_\zeta = 1 + p_\zeta(x), \quad p_\zeta(x) = \cos^2(\delta_p)(x/R), \quad (12a)$$

$$h_\zeta^2 = 1 + q_\zeta(x), \quad q_\zeta(x) = \cos^2(\delta_p)(2/R)x. \quad (12b)$$

The Laplace transform

$$\tilde{a}(s) = \mathcal{L}\{a(\zeta)\} = \int_{\zeta=0}^{\infty} a(\zeta)e^{-s\zeta}d\zeta \quad (13)$$

is applied on the ζ-dimension, where $a(\zeta)$ represents any ζ-dependent variables and $\zeta = (R\phi_c)/\cos(\delta_p)$. Laplace transform on the differential

wave equations is needed to obtain the wave equations (and thus also the output fields) that are expressed directly as functions of the transmitted fields at the entrance of the waveguide at $\zeta = 0^+$. Thus, the Laplace transform is necessary to obtain the comfortable and simple input-output connections of the fields.

Let us introduce the main steps, in detail. By substitution of Eqs. (8a)–(8c) into Eqs. (10a) and (10b), by using the Laplace transform (13), and multiply by h_ζ^2, Eqs. (7a) are described in the Laplace transform domain in the form

$$h_\zeta^2\left(\nabla_\perp^2+\frac{s^2}{h_\zeta^2}+k^2\right)\tilde{E}_x+h_\zeta^2\partial_x\left(\tilde{E}_x g_x+\tilde{E}_y g_y\right)+h_\zeta\frac{1}{R}\cos^2(\delta_p)\partial_x\left(\tilde{E}_x\right)$$
$$-\frac{2}{R}\cos^2(\delta_p)s\tilde{E}_\zeta=\left(sE_{x_0}+E'_{x_0}\right)-\frac{2}{R}\cos^2(\delta_p)E_{\zeta_0} \tag{14a}$$

$$h_\zeta^2\left(\nabla_\perp^2+\frac{s^2}{h_\zeta^2}+k^2\right)\tilde{E}_y+h_\zeta^2\partial_y\left(\tilde{E}_x g_x+\tilde{E}_y g_y\right)+h_\zeta\frac{1}{R}\cos^2(\delta_p)\partial_x\left(\tilde{E}_y\right)$$
$$=\left(sE_{y_0}+E'_{y_0}\right) \tag{14b}$$

$$h_\zeta^2\left(\nabla_\perp^2+\frac{s^2}{h_\zeta^2}+k^2\right)\tilde{E}_\zeta+sh_\zeta^2\left(\tilde{E}_x g_x+\tilde{E}_y g_y\right)+h_\zeta\frac{1}{R}\cos^2(\delta_p)\partial_x\left(\tilde{E}_\zeta\right)$$
$$+\frac{2}{R}\cos^2(\delta_p)s\tilde{E}_x=\left(sE_{\zeta_0}+E'_{\zeta_0}\right)+\frac{2}{R}\cos^2(\delta_p)E_{x_0}+h_\zeta^2\left(E_{x_0}g_x+E_{y_0}g_y\right), \tag{14c}$$

where the transverse Laplacian operator is defined according to (11), E_{x_0}, E_{y_0}, $E_{\zeta 0}$ are the initial values of the corresponding fields at $\zeta = 0$, i.e., $E_{x_0} = E_x(x, y, \zeta = 0)$ and $E'_{x_0} = \frac{\partial}{\partial\zeta}E_x(x, y, \zeta)|_{\zeta=0}$.

A Fourier transform is applied on the transverse dimension

$$\bar{g}(k_x, k_y) = \mathcal{F}\{g(x, y)\} = \int_x\int_y g(x, y)e^{-jk_x x-jk_y y}dxdy, \tag{15}$$

and the differential equation (14a) is transformed to an algebraic form

in the (ω, s, k_x, k_y) space, as follows

$$k_\zeta^2\bar{\bar{E}}_x + s^2\bar{\bar{E}}_x + k_o^2\chi_o\bar{g} * \bar{\bar{E}}_x + jk_x\left(\bar{g}_x * \bar{\bar{E}}_x + \bar{g}_y * \bar{\bar{E}}_y\right) - \frac{2}{R}\cos^2(\delta_p)s\bar{\bar{E}}_\zeta$$
$$+\bar{q}_\zeta*\left(k_\zeta^2\right)\bar{\bar{E}}_x + k_o^2\chi_o\bar{q}_\zeta*\left(\bar{g} * \bar{\bar{E}}_x\right) + j\bar{q}_\zeta*\left[k_x\left(\bar{g}_x * \bar{\bar{E}}_x + \bar{g}_y * \bar{\bar{E}}_y\right)\right]$$
$$+\frac{1}{R}\cos^2(\delta_p)\left(jk_x\right)\bar{\bar{E}}_x + \frac{1}{R}\cos^2(\delta_p)j\bar{p}_\zeta*\left(k_x\bar{\bar{E}}_x\right) = \left(s\bar{E}_{x_0} + \bar{E}'_{x_0}\right)$$
$$-\frac{1}{sR}\cos^2(\delta_p)\left(s\bar{E}_{\zeta_0} + \bar{E}'_{\zeta_0}\right), \tag{16}$$

where $k_\zeta = \sqrt{k_o^2 - k_x^2 - k_y^2}$. Similarly, the other differential equations are obtained. The asterisk symbol denotes the convolution operation $\bar{g} * \bar{E} = \mathcal{F}\{g(x,y)E(x,y)\}$.

The method of images is applied to satisfy the conditions $\widehat{n}\times E = 0$ and $\widehat{n}\cdot(\bigtriangledown \times E) = 0$ on the surface of the ideal metallic waveguide walls, where $\widehat{n}$ is a unit vector perpendicular to the surface. The metric coefficient h_ζ is a function of x (Eqs. (12a) and (12b)). Thus the elements of the matrices $\mathbf{P^{(0)}}$ and $\mathbf{Q^{(0)}}$ are defined as:

$$\bar{p_\zeta}^{(o)}_{(n,m)} = \frac{1}{4ab}\int_{-a}^{a}\int_{-b}^{b} p_\zeta(x)\ \ e^{-j(n\frac{\pi}{a}x + m\frac{\pi}{b}y)}\ \ dxdy, \tag{17a}$$

$$\bar{q_\zeta}^{(o)}_{(n,m)} = \frac{1}{4ab}\int_{-a}^{a}\int_{-b}^{b} q_\zeta(x)\ \ e^{-j(n\frac{\pi}{a}x + m\frac{\pi}{b}y)}\ \ dxdy, \tag{17b}$$

and the matrices $\mathbf{P^{(1)}}$ and $\mathbf{Q^{(1)}}$ are defined as:

$$\mathbf{P^{(1)}} = \left(\mathbf{I} + \mathbf{P^{(0)}}\right),\quad \mathbf{Q^{(1)}} = \left(\mathbf{I} + \mathbf{Q^{(0)}}\right), \tag{17c}$$

where $\mathbf{I}$ is the unity matrix.

Equation (16) and similarly, the two other equations are rewritten in a matrix form as follows

$$\mathbf{K^{(0)}}E_x + \frac{k_o^2\chi_0}{2s}\mathbf{Q^{(1)}}\mathbf{G}E_x + \frac{jk_{ox}}{2s}\mathbf{Q^{(1)}}\mathbf{N}\left(\mathbf{G_x}E_x + \mathbf{G_y}E_y\right)$$
$$-\frac{1}{R}\cos^2(\delta_p)E_\zeta + \mathbf{Q^{(0)}}\mathbf{K1^{(0)}}E_x + \frac{1}{2sR}\cos^2(\delta_p)jk_{ox}\mathbf{P^{(1)}}\mathbf{N}E_x$$

$$= \hat{E}_{x_0} - \frac{1}{sR}\cos^2(\delta_p)\bar{E}_{\zeta_0}, \tag{18a}$$

$$\mathbf{K^{(0)}}E_y + \frac{k_o^2\chi_0}{2s}\mathbf{Q^{(1)}}\mathbf{G}E_y + \frac{jk_{oy}}{2s}\mathbf{Q^{(1)}}\mathbf{M}\left(\mathbf{G_x}E_x + \mathbf{G_y}E_y\right)$$

$$+\mathbf{Q^{(0)}}\mathbf{K1^{(0)}}E_y + \frac{1}{2sR}\cos^2(\delta_p)jk_{ox}\mathbf{P^{(1)}}\mathbf{N}E_y = \hat{E}_{y_0}, \tag{18b}$$

$$\mathbf{K^{(0)}}E_\zeta + \frac{k_o^2\chi_0}{2s}\mathbf{Q^{(1)}}\mathbf{G}E_\zeta + \frac{1}{2}\mathbf{Q^{(1)}}\left(\mathbf{G_x}E_x + \mathbf{G_y}E_y\right) + \frac{1}{R}\cos^2(\delta_p)E_x$$

$$+\mathbf{Q^{(0)}}\mathbf{K1^{(0)}}E_\zeta + \frac{1}{2sR}\cos^2(\delta_p)jk_{ox}\mathbf{P^{(1)}}\mathbf{N}E_\zeta = \hat{E}_{\zeta_0} + \frac{1}{sR}\cos^2(\delta_p)E_{x_0}$$

$$+\frac{1}{2s}\mathbf{Q^{(1)}}\left(\mathbf{G_x}E_{x_0} + \mathbf{G_y}E_{y_0}\right), \tag{18c}$$

where the initial-value vectors, $\hat{E}_{x_0}$, $\hat{E}_{y_0}$, and $\hat{E}_{\zeta_0}$ are defined from the terms $(s\bar{E}_{x_0} + \bar{E}'_{x_0})/2s$, $(s\bar{E}_{y_0} + \bar{E}'_{y_0})/2s$, and $(s\bar{E}_{\zeta_0} + \bar{E}'_{\zeta_0})/2s$, respectively.

The elements of the diagonal matrices $\mathbf{K^{(0)}}$, $\mathbf{M}$, $\mathbf{N}$ and $\mathbf{K^{(1)}}$ are defined as

$$K^{(0)}{}_{(n,m)(n',m')} = \left\{\left[k_o^2 - (n\pi/a)^2 - (m\pi/b)^2 + s^2\right]/2s\right\}\delta_{nn'}\delta_{mm'}, \tag{19a}$$

$$M_{(n,m)(n',m')} = m\delta_{nn'}\delta_{mm'}, \tag{19b}$$

$$N_{(n,m)(n',m')} = n\delta_{nn'}\delta_{mm'}, \tag{19c}$$

$$K^{(1)}{}_{(n,m)(n',m')} = \left\{\left[k_o^2 - (n\pi/a)^2 - (m\pi/b)^2\right]/2s\right\}\delta_{nn'}\delta_{mm'}. \tag{19d}$$

where $\delta_{nn'}$ and $\delta_{mm'}$ are the Kronecker delta functions.

The modified wave-number matrices are defined as

$$\mathbf{D_x} \equiv \mathbf{K^{(0)}} + \mathbf{Q^{(0)}}\mathbf{K1^{(0)}} + \frac{k_o^2\chi_0}{2s}\mathbf{Q^{(1)}}\mathbf{G} + \frac{jk_{ox}}{2s}\mathbf{Q^{(1)}}\mathbf{N}\mathbf{G_x}$$
$$+\frac{1}{2sR}\cos^2(\delta_p)jk_{ox}\mathbf{P^{(1)}}\mathbf{N}, \tag{20a}$$

$$\mathbf{D_y} \equiv \mathbf{K^{(0)}} + \mathbf{Q^{(0)}}\mathbf{K1^{(0)}} + \frac{k_o^2\chi_0}{2s}\mathbf{Q^{(1)}}\mathbf{G} + \frac{1}{2sR}\cos^2(\delta_p)jk_{ox}\mathbf{P^{(1)}}\mathbf{N}$$
$$+\frac{jk_{oy}}{2s}\mathbf{Q^{(1)}}\mathbf{M}\mathbf{G_y}, \tag{20b}$$

$$\mathbf{D_\zeta} \equiv \mathbf{K^{(0)}} + \mathbf{Q^{(0)}}\mathbf{K1^{(0)}} + \frac{k_o^2\chi_0}{2s}\mathbf{Q^{(1)}}\mathbf{G} + \frac{1}{2sR}\cos^2(\delta_p)jk_{ox}\mathbf{P^{(1)}}\mathbf{N}. \tag{20c}$$

Thus, Eqs. (18(a–c)) result in

$$\mathbf{D_x}E_x = \hat{E}_{x_0} - \frac{jk_{ox}}{2s}\mathbf{Q^{(1)}}\mathbf{N}\mathbf{G_y}E_y - \frac{1}{sR}\cos^2(\delta_p)E_{\zeta_0} + \frac{1}{R}\cos^2(\delta_p)E_\zeta, \tag{21a}$$

$$\mathbf{D_y}E_y = \hat{E}_{y_0} - \frac{jk_{oy}}{2s}\mathbf{Q^{(1)}}\mathbf{M}\mathbf{G_x}E_x, \tag{21b}$$

$$\mathbf{D}_\zeta E_\zeta = \hat{E}_{\zeta_0} + \frac{1}{2s}\mathbf{Q^{(1)}}\left(\mathbf{G_x}E_{x_0} + \mathbf{G_y}E_{y_0}\right) - \frac{1}{2}\mathbf{Q^{(1)}}\left(\mathbf{G_x}E_x + \mathbf{G_y}E_y\right) + \frac{1}{sR}\cos^2(\delta_p)E_{x_0} - \frac{1}{R}\cos^2(\delta_p)E_x. \tag{21c}$$

After some algebraic steps, the components of the electric field are formulated as follows:

$$\begin{aligned} E_x = &\left\{\mathbf{D_x} + \alpha_1\mathbf{Q}^{(1)}\mathbf{M}_1\mathbf{Q}^{(1)}\mathbf{M}_2 + \frac{1}{R}\cos^2(\delta_p)\mathbf{D}_\zeta{}^{-1}\right. \\ &\left.\left(-\frac{1}{2}\mathbf{Q}^{(1)}\mathbf{G_x} + \frac{1}{2}\alpha_2\mathbf{Q}^{(1)}\mathbf{M}_3\mathbf{Q}^{(1)}\mathbf{M}_2 - \frac{1}{R}\cos^2(\delta_p)\mathbf{I}\right)\right\}^{-1} \\ &\left(\hat{E}_{x_0} - \frac{1}{sR}\cos^2(\delta_p)E_{\zeta_0} - \alpha_3\mathbf{Q}^{(1)}\mathbf{M}_1\hat{E}_{y_0} + \frac{1}{R}\cos^2(\delta_p)\mathbf{D}_\zeta{}^{-1}\right. \\ &\left(\hat{E}_{\zeta_0} + \frac{1}{sR}\cos^2(\delta_p)E_{x_0} + \frac{1}{2s}\mathbf{Q}^{(1)}(\mathbf{G_x}E_{x_0} + \mathbf{G_y}E_{y_0})\right. \\ &\left.\left. - \frac{1}{2}\mathbf{Q}^{(1)}\mathbf{M}_3\hat{E}_{y_0}\right)\right), \end{aligned} \tag{22a}$$

$$E_y = \mathbf{D_y}{}^{-1}\left(\hat{E}_{y_0} - \frac{jk_{oy}}{2s}\mathbf{Q}^{(1)}\mathbf{M}\mathbf{G_x}E_x\right), \tag{22b}$$

$$E_\zeta = \mathbf{D}_\zeta{}^{-1}\left\{\hat{E}_{\zeta_0} + \frac{1}{2s}\mathbf{Q}^{(1)}\left(\mathbf{G_x}E_{x_0} + \mathbf{G_y}E_{y_0}\right) - \frac{1}{2}\mathbf{Q}^{(1)}\left(\mathbf{G_x}E_x + \mathbf{G_y}E_y\right) - \frac{1}{R}\cos^2(\delta_p)E_x + \frac{1}{sR}\cos^2(\delta_p)E_{x_0}\right\}, \tag{22c}$$

where:

$$\alpha_1 = \frac{k_{ox}k_{oy}}{4s^2}, \quad \alpha_2 = \frac{jk_{oy}}{2s}, \quad \alpha_3 = \frac{jk_{ox}}{2s},$$
$$\mathbf{M}_1 = \mathbf{N}\mathbf{G_y}\mathbf{D_y}{}^{-1}, \quad \mathbf{M}_2 = \mathbf{M}\mathbf{G_x}, \quad \mathbf{M}_3 = \mathbf{G_y}\mathbf{D_y}{}^{-1}.$$

These equations describe the transfer relations between the spatial spectrum components of the output and input waves in the dielectric

waveguide. Similarly, the other components of the magnetic field are obtained. The transverse field profiles are computed by the inverse Laplace and Fourier transforms, as follows

$$E_y(x,y,\zeta) = \sum_n \sum_m \int_{\sigma-j_\infty}^{\sigma+j_\infty} E_y(n,m,s) e^{jnk_{ox}x + jmk_{oy}y + s\zeta} ds. \quad (23a)$$

The inverse Laplace transform is performed in this study by a direct numerical integration on the s-plane by the method of Gaussian Quadrature. The integration path in the right side of the s-plane includes all the singularities, as proposed by Salzer [19, 20]

$$\int_{\sigma-j_\infty}^{\sigma+j_\infty} e^{s\zeta} E_y(s) ds = \frac{1}{\zeta} \int_{\sigma-j_\infty}^{\sigma+j_\infty} e^{p} E_y(p/\zeta) dp = \frac{1}{\zeta} \sum_{i=1}^{15} w_i E_y(s = p_i/\zeta), \quad (23b)$$

where w_i and p_i are the weights and zeros, respectively, of the orthogonal polynomials of order 15. The Laplace variable s is normalized by p_i/ζ in the integration points, where $\mathrm{Re}\,(p_i) > 0$ and all the poles should be localized in their left side on the Laplace transform domain. This approach of a direct integral transform does not require as in other methods, to deal with each singularity separately. The relation between the functions $f(t)$ and $F(p)$ is given by

$$f(t) = \frac{1}{2\pi j} \int_{\sigma-j_\infty}^{\sigma+j_\infty} e^{pt} F(p) dp. \quad (24)$$

The function $F(p)$ may be either known only numerically or too complicated for evaluating $f(t)$ by Cauchy's theorem. The function $F(p)$ behaves like a Polynomial without a constant term, in the variable $1/p$, along $(\sigma - j_\infty, \sigma + j_\infty)$. One may find $f(t)$ numerically by using new quadrature formulas (analogous to those employing the zeros of the Laguerre polynomials in the direct Laplace transform). A suitable choice of p_i yields an n-point quadrature formula that is exact when p_{2n} is any arbitrary polynomial of the $2n$(th) degree in $x \equiv 1/p$, namely,

$$\frac{1}{2\pi j} \int_{\sigma-j_\infty}^{\sigma+j_\infty} e^{p} \rho(1/p) dp = \sum_{i=1}^{n} A_i(n) \rho_{2n}(1/p_i). \quad (25)$$

In Eq. (25), $x_i \equiv 1/p_i$ are the zeros of the orthogonal polynomials where

$$\frac{1}{2\pi j} \int_{\sigma-j_\infty}^{\sigma+j_\infty} e^{p} \left(\frac{1}{p}\right) p_n \left(\frac{1}{p}\right) \left(\frac{1}{p}\right)^i dp = 0, \quad (26)$$

$i = 0, 1, \ldots, n-1$ and $A_i(n)$ correspond to the Christoffel numbers. The normalization $P_n(1/p) \equiv (4n-2)(4n-6), \ldots, 6p_n(1/p)$, for $n \geq 2$, produces all integral coefficients. $P_n(1/p)$ is proven [19, 20] to be $(-1)^n e^{-p} p^n d^n(e^p/p^n)/dp^n$.

The numerical table gives us the values of the reciprocals of the zeros of $P_n(x)$ or $p_i(n)$, the zeros of $P_n(x)$, or $1/{p_i}^n$, and the corresponding Christoffel numbers $A_i(n)$. By using these quantities in the quadrature formula that represents in Eq. (25), then the Christoffel numbers are given by

$$A_i(n) \equiv \frac{1}{2\pi j} \int_{\sigma - j\infty}^{\sigma + j\infty} e^p L_i(n+1) \left(\frac{1}{p}\right) dp. \tag{27}$$

A sufficient condition for Eq. (27) to hold is obviously the orthogonality of $(1/p)p_n(1/p)$ with respect to any arbitrary $\rho(1/p)$ (see Eq. (26)).

The points $1/p_i$ are denoted by $1/(p_i)^n$ and they are the zeros of a certain set of the orthogonal polynomials in the variable $1/p$. By using these quantities in the quadrature formula we can obtain theoretically the exact accuracy for any polynomial in $1/p$ up to the 16(th) degree.

The ζ component of the average-power density of the complex Poynting vector is given by

$$S_{av} = \frac{1}{2} \mathrm{Re} \left\{ E_x {H_y}^* - E_y {H_x}^* \right\}, \tag{28}$$

where the asterisk indicates the complex conjugate. The active power is equal to the real part of the complex Poynting vector. The total average-power transmitted along the guide in the ζ direction is given by a double integral of Eq. (28). A Fortran code is developed using NAG subroutines [21]. Several examples computed on a Unix system are presented in the next section.

It is very interesting to compare between the mode model methods for wave propagation in the waveguide with a rectangular cross section [15, 16] and in the waveguide with a circular cross section [17, 18]. These the two kinds of the different methods enable us to solve practical problems with different boundary conditions. Let us introduce the similar main points. The calculations in all the two above methods are based on using Laplace and Fourier transforms, and the output fields are computed by the inverse Laplace and Fourier transforms. Laplace transform on the differential wave equations is needed to obtain the wave equations (and thus also the output fields) that are expressed directly as functions of the transmitted fields at the entrance of the waveguide at $\zeta = 0^+$. Thus, the Laplace

transform is necessary to obtain the comfortable and simple input-output connections of the fields. The objective in all the methods [15] and [17, 18] was to develop a mode model in order to provide a numerical tool for the calculation of the output fields for a curved waveguide.

The technique of the methods is quite different. The technique for a rectangular cross section is based on Fourier coefficients of the transverse dielectric profile and those of the input wave profile. On the other hand, the technique for a circular cross section was based on the development of the longitudinal components of the fields into Fourier-Bessel series. The transverse components of the fields were expressed as functions of the longitudinal components in the Laplace plane and were obtained by using the inverse Laplace transform.

4. NUMERICAL RESULTS

This section presents several examples which demonstrate features of the proposed mode model derived in the previous section. The method of this model is based on Fourier coefficients, thus the accuracy of the method is dependent on the number of the modes in the system. Further we assume $N = M$. The convergence of the solution is verified by the criterion

$$C(N) \equiv \log \left\{ \frac{\max(\left|S_{av}^{N+2} - S_{av}^{N}\right|)}{\left|\max\left(S_{av}^{N+2}\right) - \min\left(S_{av}^{N}\right)\right|} \right\}, \quad N \geq 1. \tag{29}$$

where the number of the modes is equal to $(2N + 1)^2$. The order N determines the accuracy of the solution. If the value of the criterion is less then -2, then the numerical solution is well converged.

A comparison with the known transcendental equation [22] is needed, in order to examine the validity of the theoretical model. We derive the transcendental equation and the field E_y by the potentials for TE_{10} mode. We confirm the validity of our model by comparison of the numerically computed results with the results based on the transcendental equation for a dielectric slab (Fig. 4). The derivation is given in detail in Appendix C.

Let us compare the theoretical model with the known analytical theory. For the given dimensions a and d, we find the values Λ and Ω according to the next transcendental equation for a dielectric slab (Fig. 4). According to our theoretical model we can calculate $E_{y_0}(n, m)$

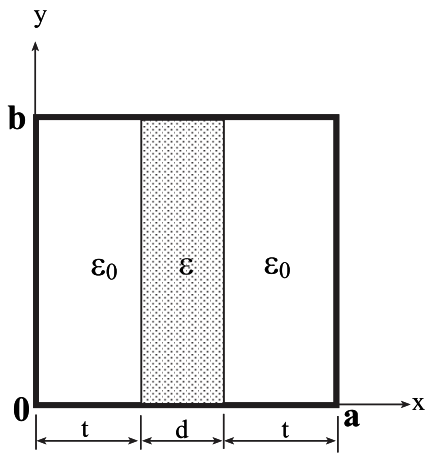

Figure 4. A dielectric slab in a rectangular metallic waveguide.

and $g(n,m)$ as follows:

$$E_{y_0}(n,m) = \frac{1}{4ab}\int_{-a}^{a}\int_{-b}^{b} E_y(x,y,z=0)e^{-j(n\frac{\pi}{a}x+m\frac{\pi}{b}y)}dxdy,$$

and

$$g(n,m) = \frac{1}{4ab}\int_{-a}^{a}\int_{-b}^{b} g(x,y)e^{-j(n\frac{\pi}{a}x+m\frac{\pi}{b}y)}dxdy.$$

The known solution for the dielectric slab modes based on transcendental equation [22] is given as follows

$$\begin{cases} E_{y1} = j\dfrac{k_z}{\epsilon_0}\sin(\nu x) & 0 < x < t \\ E_{y2} = j\dfrac{k_z}{\epsilon_0}\dfrac{\sin(\nu t)}{\cos(\mu(t-a/2))}\cos\left[\mu(x-a/2)\right] & t < x < t+d \\ E_{y3} = j\dfrac{k_z}{\epsilon_0}\sin\left[\nu(a-x)\right] & t+d < x < a \end{cases}, \quad (30)$$

where $\nu \equiv \sqrt{k_o^2 - k_z^2}$ and $\mu \equiv \sqrt{\epsilon_r k_o^2 - k_z^2}$ result from the transcendental equation

$$\left(\frac{a}{d}-1\right)\frac{d\mu}{2}\tan\left(\frac{d\mu}{2}\right) - (t\nu)\cot(t\nu) = 0.$$

Equations (30) were substituted as the initial fields into the Eq. (22b) at $z = 0^+$ in the practical case of the straight waveguide (by letting $R \to \infty$ or by taking $\delta_p = \pi/2$) with the symmetrical slab profile (Fig. 4). The result of the comparison between the theoretical model with the known solution [22] is shown in Fig. 5(a), where $\epsilon_r = 9$, $d = 3.3\,\text{mm}$, and $\lambda = 6.9\,\text{cm}$. The convergence of the numerical results as a function of the matrix order is shown in Fig. 5(b). The comparison is demonstrated for every order ($N = 1$, 3, 5, 7, and 9). The order N determines the accuracy of the solution. The convergence of the solution is verified by the criterion (29) for the E_y component of the fields (instead of S_{av}). If the value of the criterion is less then -2, then the numerical solution is well converged. When N increases, then $E_y(N)$ approaches E_y. The value of the criterion between $N = 7$ and $N = 9$ is equal to $-2.38 \simeq -2$, namely, a hundredth part. The comparison between the theoretical mode-model and the known model [22] has shown good agreement.

Note that we have two ways to compare between the results of our mode model with the other methods. The first way is to compare between the results of the output fields for every order ($N = 1$, 3, 5, 7, and 9) with the final solution of the known method. The second way is to compare between the results of the output fields (according to our model) for every two orders ($N = 1$, 3, $N = 3$, 5, $N = 5$, 7, and $N = 7$, 9), until our numerical solution is well converged. This way is efficient in the cases that we have complicated problems that we cannot compare with the final solution of the known method.

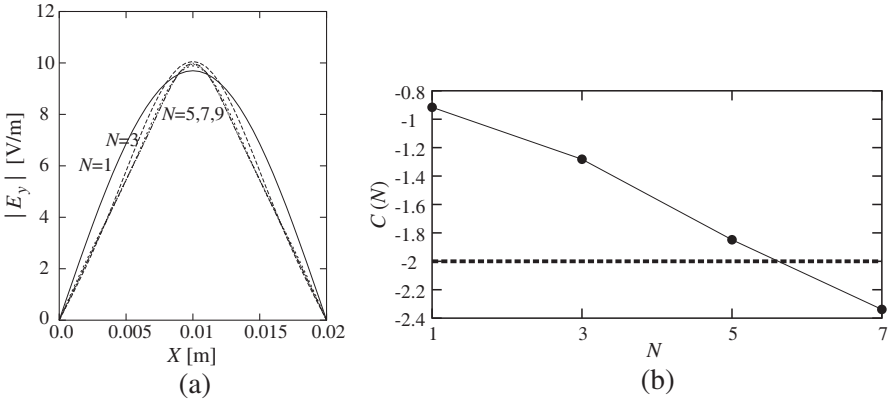

Figure 5. (a) A comparison between amplitude results of the theoretical model and the transcendental equation ($a = 2b = 2\,\text{cm}$, $d = 3.3\,\text{mm}$, $\epsilon_r = 9$, and $\lambda = 6.9\,\text{cm}$; (b) The convergence of our theoretical results.

A circular dielectric profile in a rectangular waveguide

The geometrical shape of a circular dielectric profile loaded rectangular waveguide is demonstrated in Fig. 6 for an inhomogeneous dielectric profile in the cross section. The radius of the circle is denoted as r_1 and the dimensions of the waveguide in the cross section are denoted as a and b. The refractive index of the core (dielectric profile) is greater than that of the cladding (air). Further, the next examples will demonstrate the results of the solutions in the case of a circular dielectric profile in a rectangular waveguide (Fig. 6), for $r_1 = 0.5\,\text{mm}$ and for $a = b = 2\,\text{cm}$.

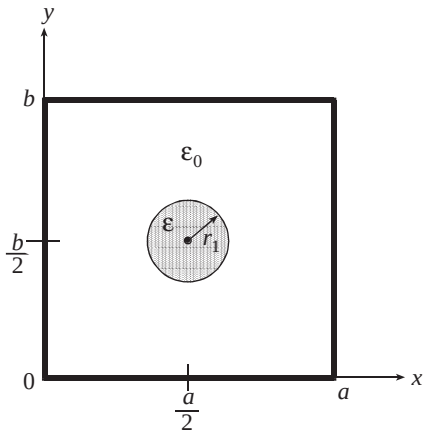

Figure 6. An example of the cross section of a dielectric profile loaded rectangular waveguide.

In order to solve discontinuous problems in the cross section, the ω_ϵ function, "cap-shaped function" [23], is used. The ω_ε function (Fig. 7) is defined as

$$\omega_\varepsilon(r) = \begin{cases} C_\varepsilon e^{-\frac{\varepsilon^2}{\varepsilon^2 - |r|^2}} & |r| \le \varepsilon, \\ 0 & |r| > \varepsilon \end{cases}$$

where the constant C_ε is chosen to satisfy $\int \omega_\varepsilon(r)dr = 1$.

The ω_ε function in the limit $\varepsilon \longrightarrow 0$ is shown in Fig. 8.

Let us assume that the center of the circle located at the point $(a/2,\, b/2)$, as shown in Fig. 6. The dielectric profile $g(x, y)$ in this case

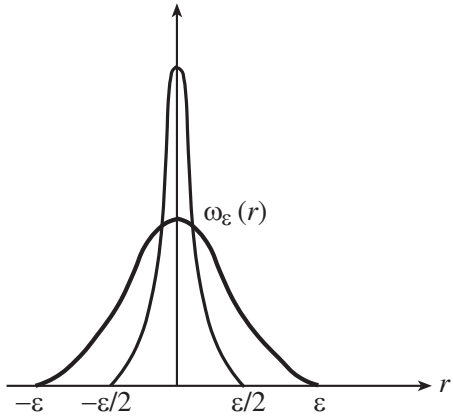

Figure 7. The ω_ε function.

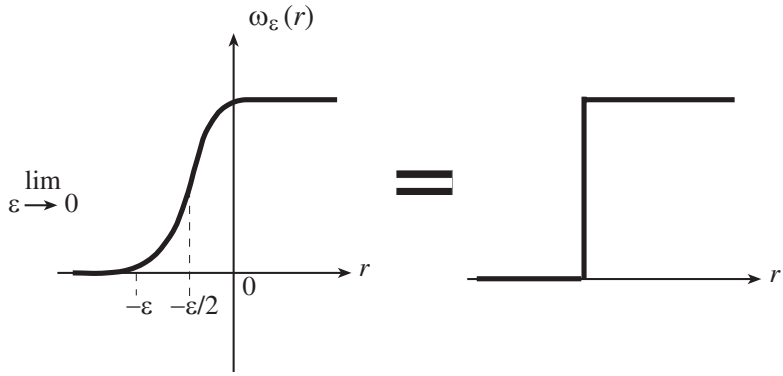

Figure 8. The ω_ε function in the limit $\varepsilon \longrightarrow 0$.

is given by

$$g(x,y)=\begin{cases} g_0 & 0 \le r < r_1 - \varepsilon_1/2 \\ g_0 \exp\left[1-\frac{{\varepsilon_1}^2}{{\varepsilon_1}^2-[r-(r_1-\varepsilon_1/2)]^2}\right] & r_1-\varepsilon_1/2 \le r < r_1+\varepsilon_1/2 \\ 0 & else \end{cases},$$

where $r=\sqrt{(x-a/2)^2+(y-b/2)^2}$.

The derivatives of the dielectric profile are defined as

$$g_x \equiv \frac{1}{\epsilon(x,y)}\frac{\partial\epsilon(x,y)}{\partial x} = \frac{\partial[\ln(1+g(x,y))]}{\partial x},$$
$$g_y \equiv \frac{1}{\epsilon(x,y)}\frac{\partial\epsilon(x,y)}{\partial y} = \frac{\partial[\ln(1+g(x,y))]}{\partial y}.$$

where $(\partial/\partial x) = (\partial/\partial r)(\partial r/\partial x)$ and $(\partial/\partial y) = (\partial/\partial r)(\partial r/\partial y)$.

Thus, the derivatives of the dielectric profile are calculated as follow

$$g_x = \begin{cases} 0 & 0 \le r < r_1 - \varepsilon_1/2 \\ -2g_0\cos\theta\exp\left[1-\frac{{\varepsilon_1}^2}{{\varepsilon_1}^2-[r-(r_1-\varepsilon_1/2)]^2}\right] & \\ \dfrac{[r-(r_1-\varepsilon_1/2)]{\varepsilon_1}^2}{\left\{1+g_0\exp\left[1-\frac{{\varepsilon_1}^2}{{\varepsilon_1}^2-[r-(r_1-\varepsilon_1/2)]^2}\right]\right\}} & r_1-\varepsilon_1/2 \le r < r_1-\varepsilon_1/2 \\ \left[{\varepsilon_1}^2-[r-(r_1-\varepsilon_1/2)]^2\right]^2 & \\ 0 & else \end{cases}.$$

$$g_y = \begin{cases} 0 & 0 \le r < r_1 - \varepsilon_1/2 \\ -2g_0\sin\theta\exp\left[1-\frac{{\varepsilon_1}^2}{{\varepsilon_1}^2-[r-(r_1-\varepsilon_1/2)]^2}\right] & \\ \dfrac{[r-(r_1-\varepsilon_1/2)]{\varepsilon_1}^2}{\left\{1+g_0\exp\left[1-\frac{{\varepsilon_1}^2}{{\varepsilon_1}^2-[r-(r_1-\varepsilon_1/2)]^2}\right]\right\}} & r_1-\varepsilon_1/2 \le r < r_1-\varepsilon_1/2 \\ \left[{\varepsilon_1}^2-[r-(r_1-\varepsilon_1/2)]^2\right]^2 & \\ 0 & else \end{cases}.$$

The elements of the matrices $g(n,m)$, $g_x(n,m)$ and $g_y(n,m)$ are given by

$$g(n,m) = \frac{g_0}{ab}\left\{\int_0^{2\pi}\int_0^{r_1-\epsilon/2}\cos\left[\frac{n\pi}{a}\left(r\cos\theta+\frac{a}{2}\right)\right]\cos\left[\frac{m\pi}{b}\left(r\sin\theta+\frac{b}{2}\right)\right]\right.$$
$$+\int_0^{2\pi}\int_{r_1-\epsilon/2}^{r_1+\epsilon/2}\cos\left[\frac{n\pi}{a}\left(r\cos\theta+\frac{a}{2}\right)\right]\cos\left[\frac{m\pi}{b}\left(r\sin\theta+\frac{b}{2}\right)\right]$$
$$\left.\exp\left[1-\frac{\epsilon^2}{\epsilon^2-[r-(r_1-\epsilon/2)]^2}\right]\right\} r dr d\theta$$

$$g_x(n,m) = -\frac{2g_0}{ab}\left\{\int_0^{2\pi}\int_{r_1-\epsilon/2}^{r_1+\epsilon/2} \frac{\epsilon^2[r-(r_1-\epsilon/2)]\exp\left[1-\frac{\epsilon^2}{\epsilon^2-[r-(r_1-\epsilon/2)]^2}\right]\cos\theta}{[\epsilon^2-[r-(r_1-\epsilon/2)]^2]^2\left[1+g_0\exp\left[1-\frac{\epsilon^2}{\epsilon^2-[r-(r_1-\epsilon/2)]^2}\right]\right]} \cos\left[\frac{n\pi}{a}\left(r\cos\theta+\frac{a}{2}\right)\right]\cos\left[\frac{m\pi}{b}\left(r\sin\theta+\frac{b}{2}\right)\right]\right\} r dr d\theta$$

$$g_y(n,m) = -\frac{2g_0}{ab}\left\{\int_0^{2\pi}\int_{r_1-\epsilon/2}^{r_1+\epsilon/2} \frac{\epsilon^2[r-(r_1-\epsilon/2)]\exp\left[1-\frac{\epsilon^2}{\epsilon^2-[r-(r_1-\epsilon/2)]^2}\right]\sin\theta}{[\epsilon^2-[r-(r_1-\epsilon/2)]^2]^2\left[1+g_0\exp\left[1-\frac{\epsilon^2}{\epsilon^2-[r-(r_1-\epsilon/2)]^2}\right]\right]} \cos\left[\frac{n\pi}{a}\left(r\cos\theta+\frac{a}{2}\right)\right]\cos\left[\frac{m\pi}{b}\left(r\sin\theta+\frac{b}{2}\right)\right]\right\} r dr d\theta$$

where $r = \sqrt{(x-a/2)^2+(y-b/2)^2}$.

Figure 9 demonstrates the influence of the step's angle (δ_p) and the radius of the cylinder (R) on the radius of curvature of the helix (ρ) along the ζ-axis of the helix. Three results are demonstrated for three values of δ_p ($\delta_p = 0,\ 0.4,\ 0.8$). For an arbitrary value of radius of cylinder, the radius of curvature of the helix is large for large values of the step's angle and decreases with decreasing the value of δ_p. On the other hand, for an arbitrary value of the step's angle, the radius of curvature of the helix is large for large values of the radius of the cylinder, and decreases with decreasing the value of the radius of the cylinder.

The main contribution of this paper is demonstrated in Fig. 10, in order to understand the influence of the step's angle (δ_p) and the radius of the cylinder (R) on the output power transmission. The output fields are dependent on the input wave profile (TE_{10} mode) and the dielectric profile. Six results are demonstrated for six values of δ_p ($\delta_p = 0,\ 0.4,\ 0.7,\ 0.8,\ 0.9,\ 1.0$), where $\zeta = 15\,\text{cm}$, $a = b = 2\,\text{cm}$, $r_1 = 0.5\,\text{mm}$, $\lambda = 3.75\,\text{cm}$, and $\epsilon_r = 10$, where the waveguide's cross section is given in Fig. 6. For an arbitrary value of R, the output power transmission is large for large values of δ_p and decreases with decreasing the value of δ_p. On the other hand, for an arbitrary value of δ_p, the output power transmission is large for large values of R and decreases with decreasing the value of R. Note that for small values of the step's angle, the radius of curvature of the helical waveguide can

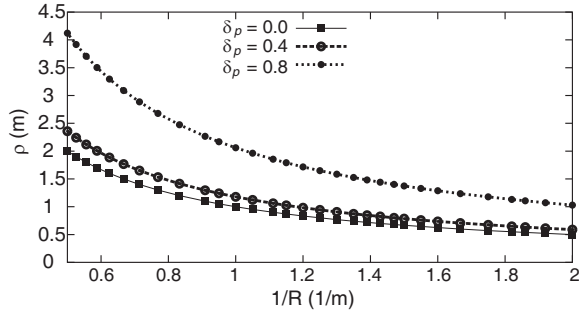

Figure 9. The radius of curvature of the helix along the ζ-axis of the helix as a function of $1/R$, where R is the radius of the cylinder. Three results are demonstrated for three values of δ_p ($\delta_p = 0$, 0.4, 0.8).

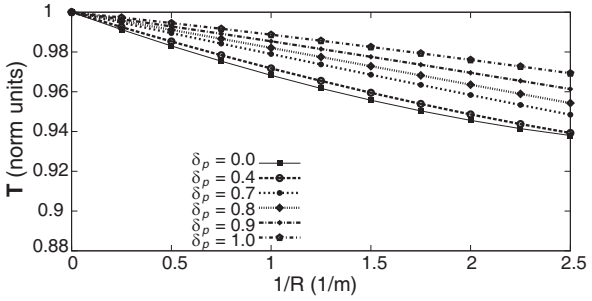

Figure 10. The results of the output power transmission as a function of $1/R$, where R is the radius of the cylinder. Six results are demonstrated for six values of δ_p ($\delta_p = 0.0$, 0.4, 0.7, 0.8, 0.9, 1.0), where $a = 20\,\text{mm}$, $b = 20\,\text{mm}$, $r_1 = 0.5\,\text{mm}$, and $\epsilon_r = 10$.

be approximated by the radius of the cylinder. In this case, the output power transmission is large for small values of the bending ($1/R$), and decreases with increasing the bending. Thus, this model can be a useful tool to find the parameters (δ_p and R) which will give us the improved results (output power transmission) of the curved waveguide in the cases of space curved waveguides.

Figures 11(a)–(d) show the results of the output power density (S_{av}) as functions of the step's angle (δ_p= 1) and the radius of the cylinder ($R = 0.5\,\text{m}$). The other parameters are: $\zeta = 15\,\text{cm}$, $a = b = 2\,\text{cm}$, $r_1 = 0.5\,\text{mm}$, $\lambda = 3.75\,\text{cm}$. The output fields are dependent on the input wave profile (TE_{10} mode) and the dielectric profile (Fig. 6). Fig. 12(a) shows the output amplitude and the Gaussian shape of

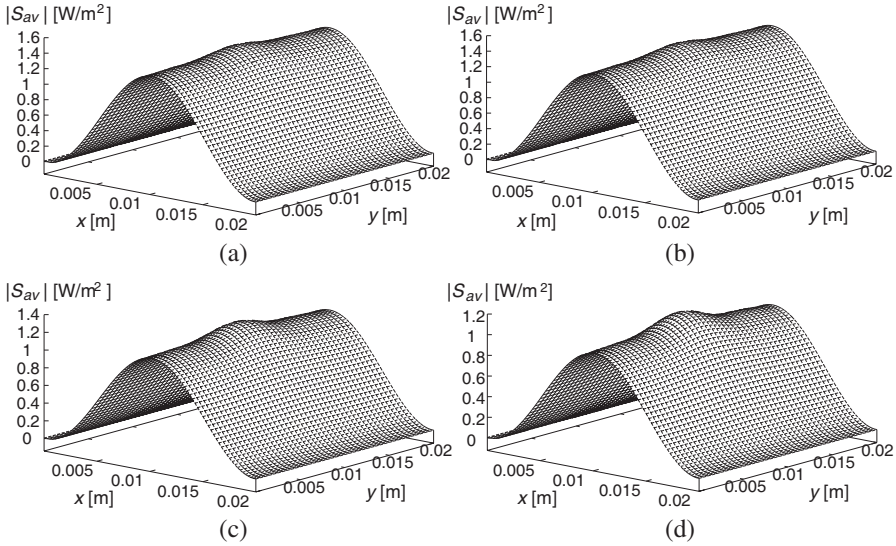

Figure 11. The results of the output power density as functions of the step's angle ($\delta_p = 1$) and the radius of the cylinder ($R = 0.5\,\mathrm{m}$), where $\zeta = 15\,\mathrm{cm}$, $a = b = 2\,\mathrm{cm}$, $r_1 = 0.5\,\mathrm{mm}$, $\lambda = 3.75\,\mathrm{cm}$: (a) $\epsilon_r = 5$; (b) $\epsilon_r = 6$; (c) $\epsilon_r = 8$; (d) $\epsilon_r = 10$.

the central peak in the same cross section of Figs. 11(a)–(d), where $y = b/2 = 1\,\mathrm{cm}$, and for five values of ε_r =2, 5, 6, 8, and 10, respectively. By changing the value of the parameter ϵ_r of the core in the cross section (Fig. 6) with regard to the cladding (air) from 2 to 10, the output transverse profile of the power density (S_{av}) is changed. For small values of ϵ_r (e.g., $\epsilon_r = 2$) the half-sine (TE_{10}) shape of the output power density appears (Fig. 11(a)), with a little influence of the Gaussian shape in the center of the output profile. On the other hand, for large values of ϵ_r (e.g., ϵ_r=10) the Gaussian shape of the output power density appears in the center of the output profile (Fig. 11(d)), with a little influence of the half-sine (TE_{10}) shape in the center of the output profile. By increasing only the parameter ϵ_r from 2 to 10, the result of the output power density shows a Gaussian shape and the amplitude of the output power density is changed from 1.6 W/m^2 to 1 W/m^2, as shown in Fig. 12(a). In this case, the output Gaussian profile increases with increasing the value of ϵ_r. These examples demonstrate the influence of the dielectric profile for an inhomogeneous cross section, for arbitrary step's angle and the radius of the cylinder of the helical waveguide.

Figure 12(b) shows an example for the output profiles with ϵ_r =

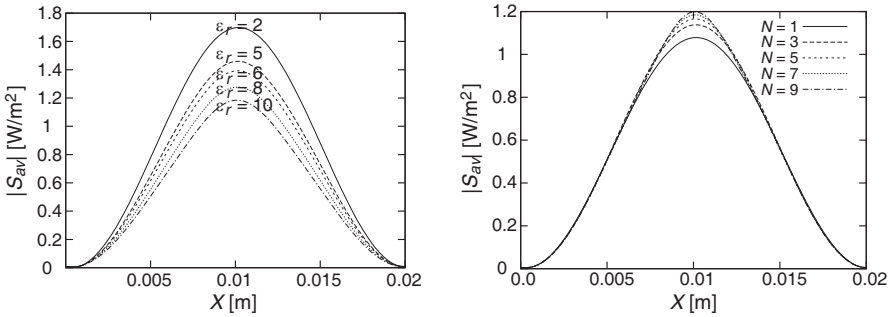

Figure 12. (a) The output amplitude and the Gaussian shape of the central peak in the same cross section of Figs. 11(a)–(d) where $y = b/2 = 1\,\text{cm}$. The output modal profile is given for the step's angle ($\delta_p = 1$) and the radius of the cylinder ($R = 0.5\,\text{m}$), where $\zeta = 15\,\text{cm}$, $a = b = 2\,\text{cm}$, $r_1 = 0.5\,\text{mm}$, $\lambda = 3.75\,\text{cm}$, and for different values of ϵ_r. (b) The output profile for $N = 1$, 3, 5, 7 and 9, where $\epsilon_r = 10$.

10, and for the same other parameters of Figs. 11(a)–(d) and 12(a). The output results are demonstrated for every order ($N = 1, 3, 5, 7,$ and 9). By increasing only the parameter of the order from $N = 1$ to $N = 9$, then the output profile approaches to the final output profile.

5. CONCLUSIONS

This paper presents a rigorous approach for the propagation of electromagnetic (EM) fields along a helical waveguide with arbitrary profiles in the rectangular cross section. The main objective was to develop a mode model to provide a numerical tool for the calculation of the output fields, output power density, and output power transmission for an arbitrary step's angle (δ_p) and the radius of the cylinder (R) of the helical waveguide. Thus, the method [15] was generalized from the curved dielectric waveguide (approximately a plane curve) with a rectangular cross section to a helical waveguide (a space curved waveguide for an arbitrary value of the step's angle of the helical waveguide) with a rectangular cross section. Another objective was to demonstrate the ability of the model to solve practical problems with inhomogeneous dielectric profiles.

The calculations are based on using Laplace and Fourier transforms, and the output fields are computed by the inverse Laplace and Fourier transforms. Laplace transform on the differential wave

equations is needed to obtain the wave equations (and thus also the output fields) that are expressed directly as functions of the transmitted fields at the entrance of the waveguide at $\zeta = 0^+$. Thus, the Laplace transform is necessary to obtain the comfortable and simple input-output connections of the fields.

The main contribution of this paper is demonstrated in Fig. 10, in order to understand the influence of the step's angle (δ_p) and the radius of the cylinder (R) on the output power transmission. Six results are demonstrated for six values of δ_p ($\delta_p = 0$, 0.4, 0.7, 0.8, 0.9, 1.0), where $\zeta = 15\,\text{cm}$, $a = b = 2\,\text{cm}$, $r_1 = 0.5\,\text{mm}$, $\lambda = 3.75\,\text{cm}$, and $\epsilon_r = 10$, where the waveguide's cross section is given in Fig. 6. The output fields are dependent on the input wave profile (TE_{10} mode) and the dielectric profile (Fig. 6). For an arbitrary value of R, the output power transmission is large for large values of δ_p and decreases with decreasing the value of δ_p. On the other hand, for an arbitrary value of δ_p, the output power transmission is large for large values of R and decreases with decreasing the value of R. Note that for small values of the step's angle, the radius of curvature of the helical waveguide can be approximated by the radius of the cylinder. In this case, the output power transmission is large for small values of the bending ($1/R$), and decreases with increasing the bending.

This model can be a useful tool to find the parameters (δ_p and R) which will give us the improved results (output power transmission) of the curved waveguide in the cases of space curved waveguides. This mode model might be a useful tool for the analysis of continuous and discontinuous curved dielectric waveguides in the microwave and millimeter-wave regimes, for diffused optical waveguides in integrated optics.

APPENDIX A.

By using the Serret-Frenet relations for a spatial curve, we can find the curvature (κ) and the torsion (τ) for each spatial curve that is characterized by y = constant and x = constant for each pair (x, y) in the range. This is achieved by using the helical transformation introduced in Eq. (1).

The location vector for the helical transformation of the coordinates (1) is given by

$$\begin{aligned}\mathbf{r} = &\left((R+x)\cos(\phi_c) + y\sin(\delta_p)\sin(\phi_c)\right)\hat{i}\\ &+\left((R+x)\sin(\phi_c) - y\sin(\delta_p)\cos(\phi_c)\right)\hat{j}\\ &+\left(y\cos(\delta_p) + R\phi_c\tan(\delta_p)\right)\hat{k}, \qquad \text{(A1)}\end{aligned}$$

where $\phi_c = (\zeta/R)\cos(\delta_p)$, R is the radius of the cylinder, and (x, y) are the parameters of the cross section.

The tangent vector is given by $\mathbf{T} = (d\mathbf{r}/d\zeta) = (d\mathbf{r}/d\phi_c)/(d\zeta/d\phi_c)$. The normal vector is given by $\mathbf{N} = (1/\kappa)(d\mathbf{T}/d\zeta)$, and the binormal vector is given by $\mathbf{B} = \mathbf{T} \times \mathbf{N}$.

The rate of the change of the tangent vector related to the parameter ζ measurses the curvature, and is given by $d\mathbf{T}/d\zeta = (d\mathbf{T}/d\phi_c)/(d\zeta/d\phi_c)$.

The curvature of the helix is constant for constant values of the radius of the cylinder (R), the step's angle (δ_p) and the parameters (x, y) of the cross section. The curvature is given by the first Serret-Frenet equation of a curve $r(\zeta)$ in the space according to $d\mathbf{T}/d\zeta = \kappa\mathbf{N}$. Thus, the curvature is

$$\kappa = \left|\frac{d\mathbf{T}}{d\zeta}\right| = \frac{\sqrt{1 + C_t}}{R(1 + \tan^2(\delta_p) + C_t)}, \tag{A2}$$

where

$$C_t = \frac{x^2}{R^2} + 2\frac{x}{R} + \frac{y^2}{R^2}\sin^2(\delta_p),$$

and the radius of curvature is given by $\rho = 1/\kappa$.

The rate of the change of the binormal vector related to the parameter ζ measurses the torsion, and is given by $d\mathbf{B}/d\zeta = (d\mathbf{B}/d\phi_c)/(d\zeta/d\phi_c)$.

The torsion of the helix is constant for constant values of the radius of the cylinder (R), the step's angle (δ_p) and the parameters (x, y) of the cross section. The torsion is given by the second Serret-Frenet equation of a curve $r(\zeta)$ in the space according to $d\mathbf{B}/d\zeta = -\tau\mathrm{N}$. Thus, the torsion is

$$\tau = \left|\frac{d\mathbf{B}}{d\zeta}\right| = \frac{\tan\delta_p}{R(1 + \tan^2(\delta_p) + C_t)}, \tag{A3}$$

where C_t is given above, and the radius of torsion is given by $\sigma = 1/\tau$.

APPENDIX B.

The purpose of this appendix is to show the derivation of $\nabla \cdot \mathbf{E}$ for the curved system (x, y, ζ). It is necessary to find the values of $\nabla \cdot \mathbf{E}$, $\nabla(\nabla \cdot \mathbf{E})$, $\nabla \times \mathbf{E}$, and $\nabla \times (\nabla \times \mathbf{E})$ in the following equation:

$$\nabla^2\mathbf{E} = \nabla(\nabla \cdot \mathbf{E}) - \nabla \times (\nabla \times \mathbf{E}),$$

that are dependent on the metric coefficients $h_x = 1$, $h_y = 1$, $h_\zeta = 1+(x/R)\cos^2(\delta_p)$, in the helical transformation of the coordinates with a rectangular cross section.

The expression for $\nabla \cdot \mathbf{E}$ is dependent on the metric coefficients as follows

$$\begin{aligned}\nabla \cdot \mathbf{E} = \mathrm{div}\mathbf{E} &= \frac{1}{h_x h_y h_\zeta}\left[\frac{\partial}{\partial x}\left(E_x h_y h_\zeta\right)+\frac{\partial}{\partial y}\left(h_x E_y h_\zeta\right)+\frac{\partial}{\partial \zeta}\left(h_x h_y E_\zeta\right)\right] \\ &= \frac{1}{h_\zeta}\left[\frac{\partial E_x}{\partial x}h_y h_\zeta+\frac{\partial E_y}{\partial y}h_\zeta+\frac{\partial E_\zeta}{\partial \zeta}h_y+E_x\frac{\partial}{\partial x}\left(h_y h_\zeta\right)\right].\end{aligned}$$

The components (x, y, ζ) of $\nabla(\nabla \cdot \mathbf{E})$ are given by

$$\begin{aligned}\left[\nabla\left(\nabla \cdot \mathbf{E}\right)\right]_x &= \frac{1}{h_x}\frac{\partial}{\partial x}\left[\frac{\partial E_x}{\partial x}+\frac{1}{h_y}\frac{\partial E_y}{\partial y}+\frac{1}{h_\zeta}\frac{\partial E_\zeta}{\partial \zeta}\right. \\ &\quad \left.+\frac{1}{h_y h_\zeta}\frac{\partial}{\partial x}\left(h_y h_\zeta\right)E_x+\frac{1}{h_y h_\zeta}\frac{\partial}{\partial y}\left(h_\zeta\right)E_y\right] \\ &= \frac{1}{h_x}\left[\frac{\partial^2 E_x}{\partial x^2}+\frac{1}{h_y}\frac{\partial^2 E_y}{\partial x \partial y}+\frac{1}{h_\zeta}\frac{\partial^2 E_\zeta}{\partial x \partial \zeta}+\frac{1}{h_y h_\zeta}\frac{\partial}{\partial x}\left(h_y h_\zeta\right)\frac{\partial E_x}{\partial x}\right. \\ &\quad \left.+\left[\frac{\partial}{\partial x}\left[\frac{1}{h_y h_\zeta}\frac{\partial}{\partial x}\left(h_y h_\zeta\right)\right]\right]E_x+\left[\frac{\partial}{\partial x}\frac{1}{h_\zeta}\right]\frac{\partial E_\zeta}{\partial \zeta}\right. \\ \left[\nabla\left(\nabla \cdot \mathbf{E}\right)\right]_y &= \frac{1}{h_y}\frac{\partial}{\partial y}\left[\frac{\partial E_x}{\partial x}+\frac{1}{h_y}\frac{\partial E_y}{\partial y}+\frac{1}{h_\zeta}\frac{\partial E_\zeta}{\partial \zeta}\right. \\ &\quad \left.+\frac{1}{h_y h_\zeta}\frac{\partial}{\partial x}\left(h_y h_\zeta\right)E_x+\frac{1}{h_y h_\zeta}\frac{\partial}{\partial y}\left(h_\zeta\right)E_y\right] \\ &= \frac{1}{h_y}\left[\frac{\partial^2 E_x}{\partial y \partial x}+\frac{1}{h_y}\frac{\partial^2 E_y}{\partial y^2}+\frac{1}{h_\zeta}\frac{\partial^2 E_\zeta}{\partial y \partial \zeta}\right. \\ &\quad \left.+\frac{1}{h_y h_\zeta}\frac{\partial}{\partial x}\left(h_y h_\zeta\right)\frac{\partial E_x}{\partial y}+\left[\frac{\partial}{\partial y}\frac{1}{h_\zeta}\right]\frac{\partial E_\zeta}{\partial \zeta}\right], \\ \left[\nabla\left(\nabla \cdot \mathbf{E}\right)\right]_\zeta &= \frac{1}{h_\zeta}\frac{\partial}{\partial \zeta}\left[\frac{\partial E_x}{\partial x}+\frac{1}{h_y}\frac{\partial E_y}{\partial y}+\frac{1}{h_\zeta}\frac{\partial E_\zeta}{\partial \zeta}\right. \\ &\quad \left.+\frac{1}{h_y h_\zeta}\frac{\partial}{\partial x}\left(h_y h_\zeta\right)E_x+\frac{1}{h_y h_\zeta}\frac{\partial}{\partial y}\left(h_\zeta\right)E_y\right] \\ &= \frac{1}{h_\zeta}\left[\frac{\partial^2 E_x}{\partial \zeta \partial x}+\frac{1}{h_y}\frac{\partial^2 E_y}{\partial \zeta \partial y}+\frac{1}{h_\zeta}\frac{\partial^2 E_\zeta}{\partial \zeta^2}\right. \\ &\quad \left.+\frac{1}{h_y h_\zeta}\frac{\partial}{\partial x}\left(h_y h_\zeta\right)\frac{\partial E_x}{\partial \zeta}+\frac{1}{h_y h_\zeta}\frac{\partial h_\zeta}{\partial y}\frac{\partial E_y}{\partial \zeta}\right].\end{aligned}$$

The expression for $\nabla \times \mathbf{E}$ is dependent on the metric coefficients as follows

$$\nabla \times \mathbf{E} = \text{curl}\mathbf{E} = \frac{1}{h_x h_y h_\zeta} \begin{bmatrix} h_x\widehat{x} & h_y\widehat{y} & h_\zeta\widehat{\zeta} \\ \frac{\partial}{\partial x} & \frac{\partial}{\partial y} & \frac{\partial}{\partial \zeta} \\ h_x E_x & h_y E_y & h_\zeta E_\zeta \end{bmatrix},$$

and the expression for $\nabla \times (\nabla \times \mathbf{E})$ is given by

$$\nabla \times (\nabla \times \mathbf{E}) = \frac{1}{h_x h_y h_\zeta} \begin{bmatrix} h_x\widehat{x} & h_y\widehat{y} & h_\zeta\widehat{\zeta} \\ \frac{\partial}{\partial x} & \frac{\partial}{\partial y} & \frac{\partial}{\partial \zeta} \\ h_x(\nabla \times \mathbf{E})_x & h_y(\nabla \times \mathbf{E})_y & h_\zeta(\nabla \times \mathbf{E})_\zeta \end{bmatrix}.$$

The components (x, y, ζ) of $\nabla \times (\nabla \times \mathbf{E})$ are given by

$$\begin{aligned}
[\nabla \times (\nabla \times \mathbf{E})]_x &= \frac{1}{h_y h_\zeta}\left[\frac{\partial}{\partial y}\frac{h_\zeta}{h_x h_y}\left[\frac{\partial}{\partial x}(h_y E_y) - \frac{\partial}{\partial y}(h_x E_x)\right]\right. \\
&\quad \left. - \frac{\partial}{\partial \zeta}\frac{h_y}{h_x h_\zeta}\left[\frac{\partial}{\partial \zeta}(h_x E_x) - \frac{\partial}{\partial x}(h_\zeta E_\zeta)\right]\right] \\
&= \frac{1}{h_y h_\zeta}\left[\frac{h_\zeta}{h_x h_y}\left(h_y \frac{\partial^2 E_y}{\partial x \partial y} - h_x \frac{\partial^2 E_x}{\partial y^2}\right)\right. \\
&\quad \left. - \frac{h_y}{h_x h_\zeta}\left(h_x \frac{\partial^2 E_x}{\partial \zeta^2} - h_\zeta \frac{\partial^2 E_\zeta}{\partial x \partial \zeta}\right) + \left(\frac{h_y}{h_x h_\zeta}\frac{\partial h_\zeta}{\partial x}\right)\frac{\partial E_\zeta}{\partial \zeta}\right], \\
[\nabla \times (\nabla \times \mathbf{E})]_y &= \frac{1}{h_x h_\zeta}\left[\frac{\partial}{\partial \zeta}\frac{h_x}{h_y h_\zeta}\left[\frac{\partial}{\partial y}(h_\zeta E_\zeta) - \frac{\partial}{\partial \zeta}(h_y E_y)\right]\right. \\
&\quad \left. - \frac{\partial}{\partial x}\frac{h_\zeta}{h_x h_y}\left[\frac{\partial}{\partial x}(hy E_y) - \frac{\partial}{\partial y}(h_x E_x)\right]\right] \\
&= \frac{1}{h_x h_\zeta}\left[\frac{h_x}{h_y h_\zeta}\left(h_\zeta \frac{\partial^2 E_\zeta}{\partial y \partial \zeta} - h_y \frac{\partial^2 E_y}{\partial \zeta^2}\right)\right. \\
&\quad - \frac{h_\zeta}{h_x h_y}\left(h_y \frac{\partial^2 E_y}{\partial x^2} - hx \frac{\partial^2 E_x}{\partial x \partial y}\right) \\
&\quad \left. - \left(\frac{\partial}{\partial x}\frac{h_\zeta}{h_x}\right)\frac{\partial E_y}{\partial x} + \left(\frac{\partial}{\partial x}\frac{h_\zeta}{h_y}\right)\frac{\partial E_x}{\partial y}\right] \\
[\nabla \times (\nabla \times \mathbf{E})]_\zeta &= \frac{1}{h_x h_y}\left[\frac{\partial}{\partial x}\frac{h_y}{h_x h_\zeta}\left[\frac{\partial}{\partial \zeta}(h_x E_x) - \frac{\partial}{\partial x}(h_\zeta E_\zeta)\right]\right. \\
&\quad \left. - \frac{\partial}{\partial y}\frac{h_x}{h_y h_\zeta}\left[\frac{\partial}{\partial y}(h_\zeta E_\zeta) - \frac{\partial}{\partial \zeta}(h_y E_y)\right]\right]
\end{aligned}$$

$$= \frac{1}{h_x h_y}\left[\frac{h_y}{h_x h_\zeta}\left(h_x\frac{\partial^2 E_x}{\partial x\partial\zeta} - h_\zeta\frac{\partial^2 E_\zeta}{\partial x^2}\right)\right.$$
$$- \frac{h_x}{h_y h_\zeta}\left(h_\zeta\frac{\partial^2 E_\zeta}{\partial y^2} - h_y\frac{\partial^2 E_y}{\partial y\partial\zeta}\right) + \left(\frac{\partial}{\partial x}\frac{h_y}{h_\zeta}\right)\frac{\partial E_x}{\partial\zeta}$$
$$\left. - \left(\frac{h_y}{h_x h_\zeta}\frac{\partial h_\zeta}{\partial x}\right)\frac{\partial E_\zeta}{\partial x} - \left(\frac{\partial}{\partial x}\frac{h_y}{h_x h_\zeta}\frac{\partial h_\zeta}{\partial x}\right)E_\zeta\right].$$

The final components (x, y, ζ) of $\nabla^2\mathbf{E}$ and $\nabla^2\mathbf{H}$ are given as follows

$$(\nabla^2\mathbf{E})_x = \nabla^2 E_x - \frac{1}{R^2 h_\zeta^2}\cos^2(\delta_p)E_x - 2\frac{1}{Rh_\zeta^2}\cos^2(\delta_p)\frac{\partial}{\partial\zeta}E_\zeta, \quad \text{(B1a)}$$

$$(\nabla^2\mathbf{E})_y = \nabla^2 E_y, \quad \text{(B1b)}$$

$$(\nabla^2\mathbf{E})_\zeta = \nabla^2 E_\zeta - \frac{1}{R^2 h_\zeta^2}\cos^2(\delta_p)E_\zeta + 2\frac{1}{Rh_\zeta^2}\cos^2(\delta_p)\frac{\partial}{\partial\zeta}E_x, \quad \text{(B1c)}$$

$$(\nabla^2\mathbf{H})_x = \nabla^2 H_x - \frac{1}{R^2 h_\zeta^2}\cos^2(\delta_p)H_x - 2\frac{1}{Rh_\zeta^2}\cos^2(\delta_p)\frac{\partial}{\partial\zeta}H_\zeta, \quad \text{(B1d)}$$

$$(\nabla^2\mathbf{H})_y = \nabla^2 H_y, \quad \text{(B1e)}$$

$$(\nabla^2\mathbf{H})_\zeta = \nabla^2 H_\zeta - \frac{1}{R^2 h_\zeta^2}\cos^2(\delta_p)H_\zeta + 2\frac{1}{Rh_\zeta^2}\cos^2(\delta_p)\frac{\partial}{\partial\zeta}H_x, \quad \text{(B1f)}$$

where

$$\nabla^2 = \frac{\partial^2}{\partial x^2} + \frac{\partial^2}{\partial y^2} + \frac{1}{h_\zeta^2}\frac{\partial^2}{\partial\zeta^2} + \frac{1}{Rh_\zeta}\cos^2(\delta_p)\frac{\partial}{\partial x}. \quad \text{(B2)}$$

The test-case ($R \to \infty$)

The test-case for the straight waveguide is obtained by letting $R \to \infty$. In this case $h_\zeta \to 1$, and the components of $(\nabla^2\mathbf{E})$ and $(\nabla^2\mathbf{H})$ are given as follows

$$\left(\nabla^2\mathbf{E}\right)_i = \nabla^2 E_i, \quad \left(\nabla^2\mathbf{H}\right)_i = \nabla^2 H_i,$$

where $i = x, y, z$, $\nabla^2 = \nabla_\perp^2 + \partial^2/\partial z^2$, and $\nabla_\perp^2 = \partial^2/\partial x^2 + \partial^2/\partial y^2$, as accepted.

APPENDIX C.

The derivation of the transcendental equation is given in this appendix. The potentials for TE_{10} mode (Fig. 4) are given as follows

$$\begin{cases} \Psi_1 = C_1 \sin(k_{x1}x)e^{-jk_z z} \\ \Psi_2 = \left[C_{21}\sin\left(k_{x2}\left(x-\left(\frac{a}{2}\right)\right)\right) + C_{22}\cos\left(k_{x2}\left(x-\left(\frac{a}{2}\right)\right)\right)\right] e^{-jk_z z} \\ \Psi_3 = C_3 \sin(k_{x3}(a-x))e^{-jk_z z} \end{cases},$$

where k_z is the propagation constant.

The dispersion-equations

$$\begin{cases} k_{x1}^2 + k_z^2 = \omega^2\mu_0\epsilon_0 = k_o^2 \\ k_{x3}^2 + k_z^2 = \omega^2\mu_0\epsilon_0 = k_o^2 \\ k_{x2}^2 + k_z^2 = \omega^2\mu_0\epsilon = k_o^2\epsilon_r \end{cases},$$

where $k_{x1} = k_{x3}$.

From the symmetric solutions ($C_1 = C_3$, $C_{21} = 0$) for E_y and H_z we obtain

$$E_y = -\frac{1}{\epsilon}\frac{\partial\psi}{\partial z} = jk_z\frac{1}{\epsilon}\psi, \quad H_z = \frac{1}{j\omega\mu\epsilon}\frac{\partial^2\psi}{\partial x\partial z} = -\frac{k_z}{\omega\mu\epsilon}\frac{\partial\psi}{\partial x}.$$

By the continuity request in the regions $x = t$ and $x = a-t$ (see Fig. 4) for E_y and H_z, and by division of the equations, one can obtain for the symmetric case the transcendental equation

$$\nu\cot(\nu t) = \mu\tan(\mu d/2),$$

where $\nu \equiv \sqrt{k_o^2 - k_z^2}$, $\mu \equiv \sqrt{k_o^2\epsilon_r - k_z^2}$ and $(a-2t)/2 = d/2$.

For the symmetric solution ($C_1 = C_3$, $C_{21} = 0$) we obtain

$$\begin{cases} E_{y1} = j\frac{k_z}{\epsilon_0}\sin(\nu x)e^{-jk_z z} & 0 < x < t \\ E_{y2} = j\frac{k_z}{\epsilon_0}\frac{\sin(\nu\cdot t)}{\cos(\mu(t-a/2))}\cos\left[\mu\left(x-\frac{a}{2}\right)\right]e^{-jk_z z} & t < x < t+d \\ E_{y3} = j\frac{k_z}{\epsilon_0}\sin\left[\nu(a-x)\right]e^{-jk_z z} & t+d < x < a \end{cases}.$$

The boundary conditions for the symmetric case are

$$\begin{cases} E_{y1} = j\frac{k_z}{\epsilon_0}\sin(\nu x) & 0 < x < t \\ E_{y2} = j\frac{k_z}{\epsilon_0}\frac{\sin(\nu t)}{\cos(\mu(t-a/2))}\cos\left[\mu(x-a/2)\right] & t < x < t+d \\ E_{y3} = j\frac{k_z}{\epsilon_0}\sin\left[\nu(a-x)\right] & t+d < x < a \end{cases}, \quad \text{(C1)}$$

and

$$\frac{\partial}{\partial z}E_y(x,y,z)\big|_{z=0} = -jk_zE_y(x,y,z=0).$$

Let us denote $\Lambda \equiv (d/2)\mu$ and $\Omega \equiv t\nu$. For the given dimensions a and d, we find the values Λ and Ω according to the next transcendental equation

$$\left(\frac{a}{d}-1\right)\Lambda\tan\Lambda - \Omega\cot\Omega = 0,$$

where $\Omega \neq k\pi$ and $\Lambda \neq (2k+1)(\pi/2)$.

By addition and subtraction of the equations $\nu^2 = k_o^2 - k_z^2$ and $\mu^2 = \epsilon_r k_o^2 - k_z^2$ we obtain

$$k_o = \left(\frac{(2\Lambda/d)^2 - (\Omega/t)^2}{\epsilon_r - 1}\right)^{1/2}, \quad k_z = \left(\frac{(2\Lambda/d)^2 - \epsilon_r\,(\Omega/t)^2}{\epsilon_r - 1}\right)^{1/2}.$$

REFERENCES

1. Riess, K., "Electromagnetic waves in a bent pipe of rectangular cross section," *Q. Appl. Math.*, Vol. 1, 328–333, 1944.
2. Rice, S. O., "Reflections from circular bends in a rectangular wave guides — Matrix theory," *Bell Syst. Tech. J.*, Vol. 27, 305–349, 1948.
3. Heiblum, M. and J. H. Harris, "Analysis of curved optical waveguides by conformal transformation," *IEEE J. Quantum Electron.*, Vol. 11, 75–83, 1975. Correction, Ibid., Vol. 12, 313, 1976.
4. Kawakami, S., M. Miyagi, and S. Nishida, "Bending losses of dielectric slab optical waveguide with double or multiple claddings," *Appl. Optics*, Vol. 14, 588–2597, 1975. Correction, Ibid., Vol. 15, 1681, 1976.
5. Chang, D. C. and F. S. Barnes, "Reduction of radiation loss in a curved dielectric slab waveguide," *Sci. Rept. 2 AFOSR-72-2417*, 1973.
6. Marcatily, E. A. J. and R. A. Schmeltzer, "Hollow metallic and dielectric waveguides for long distance optical transmission and lasers," *Bell Syst. Tech. J.*, Vol. 43, 1783–1809, 1964.
7. Cochran, J. A. and R. G. Pecina, "Mode propagation in continuously curved waveguides," *Radio Science*, Vol. 1, No. 6, 679–696, 1966.

8. Carle, P. L., "New accurate and simple equivalent circuit for circular *E*-plane bends in rectangular waveguide," *Electronics Letters*, Vol. 23, No. 10, 531–532, 1987.
9. Weisshaar, A., S. M. Goodnick, and V. K. Tripathi, "A rigorous and efficient method of moments solution for curved waveguide bends," *IEEE Trans. Microwave Theory Tech.*, Vol. 40, No. 12, 2200–2206, 1992.
10. Cornet, P., R. Dusséaux, and J. Chandezon, "Wave propagation in curved waveguides of rectangular cross section," *IEEE Trans. Microwave Theory Tech.*, Vol. 47, 965–972, 1999.
11. Ghosh, S., P. K. Jain, and B. N. Basu, "Fast-wave analysis of an inhomogeneously-loaded helix enclosed in a cylindrical waveguide," *Progress In Electromagnetics Research*, PIER 18, 19–43, 1998.
12. Kumar, D. and O. N. Singh II, "Elliptical and circular step-index with conducting helical windings on the core-cladding boundaries for the different winding pitch angles — A comparative modal dispersion analysis," *Progress In Electromagnetics Research*, PIER 52, 1–21, 2005.
13. Lewin, L., D. C. Chang, and E. F. Kuester, *Electromagnetic Waves and Curved Structures*, 95–113, Chap. 8, Peter Peregrinus Ltd., 1977.
14. Trang, N. T. and R. Mittra, "Field profile in a single-mode curved dielectric waveguide of rectangular cross section," *IEEE Trans. Microwave Theory Tech.*, Vol. 29, 1315–1318, 1981.
15. Menachem, Z., "Wave propagation in a curved waveguide with arbitrary dielectric transverse profiles," *Progress In Electromagnetics Research*, PIER 42, 173–192, 2003.
16. Menachem, Z. and E. Jerby, "Transfer matrix function (TMF) for wave propagation in dielectric waveguides with arbitrary transverse profiles," *IEEE Trans. Microwave Theory Tech.*, Vol. 46, 975–982, 1998.
17. Menachem, Z., N. Croitoru, and J. Aboudi, "Improved mode model for IR wave propagation in a toroidal dielectric waveguide and applications," *Opt. Eng.*, Vol. 41, 2002.
18. Menachem, Z. and M. Mond, "Infrared wave propagation in a helical waveguide with inhomogeneous cross section and applications," *Progress In Electromagnetics Research*, PIER 61, 159–192, 2006.
19. Salzer, H. E., "Orthogonal polynomials arising in the numerical evaluation of inverse Laplace transforms," *Math. Tables and Other*

Aids to Comut., Vol. 9, 164–177, 1955.

20. Salzer, H. E., "Additional formulas and tables for orthogonal polynomials originating from inversion integrals," *J. Math. Phys.*, Vol. 39, 72–86, 1961.
21. The Numerical Algorithms Group (NAG) Ltd., Wilkinson House, Oxford, UK.
22. Collin, R. E., *Foundation for Microwave Engineering*, McGraw-Hill, New York, 1996.
23. Vladimirov, V., *Equations of Mathematical Physics*, 1971.